Polyurethane/acrylic hybrid dispersions containing phosphorus reactive flame retardants as transparent coatings for wood

M. Puyadena [a], I. Etxeberria [b], L. Martin [c], A. Mugica [a], A. Agirre [d], M. Cobos [a], A. Gonzalez [a], A. Barrio [b], L. Irusta [a,*]

[a] POLYMAT, Department of Polymers and Advanced Materials: Physics, Chemistry and Technology, University of the Basque Country UPV/EHU, PO Box 1072, 20080 Donostia-San Sebastián, Spain
[b] TECNALIA, Basque Research and Technology Alliance (BRTA), Area Anardi 5, 20730 Azpeitia, Spain
[c] Macrobehaviour-Mesostructure-Nanotechnology SGIker Service, Faculty of Engineering, University of the Basque Country UPV/EHU, Plaza Europa 1, 20018 Donostia-San Sebastián, Spain
[d] POLYMAT, Department of Applied Chemistry, University of the Basque Country UPV/EHU, Tolosa hiribidea 72, 20018 Donostia-San Sebastián, Spain

ARTICLE INFO

ABSTRACT

Phosphorus modified polyurethane/acrylic hybrid dispersions were prepared for flame retardant transparent wood coatings. The polymerisation was carried out in three steps. In the first one, the polyurethane was synthesised using an acrylic monomer as solvent. The second step involved water addition that promoted the phase inversion and lastly, acrylic part was polymerised. The phosphorous compounds were covalently linked to polyurethane using a phosphorylated polyol and to the acrylic phase using an acrylic phosphate. Polymerisation was monitored by FTIR and NMR and the molar mass of the hybrids was measured by AF4 and SEC. The effects of the phosphorus in fire-retardant properties were analysed by thermogravimetry and pyrolysis combustion flow calorimetry. The introduction of phosphorus did not produce significant changes in the polymerisation process but promoted the cross-linking of the coatings. The coated wood samples maintained the transparency and good properties with the introduction of phosphorus and presented a slight reduction in the Peak Heat Release Rate measured by cone calorimeter. The action of phosphorus as a fire retardant was effective as it gave rise to significant reduction of the CO and CO_2 peaks.

1. Introduction

Waterborne polyurethanes present good film-forming abilities, as well as excellent toughness and flexibility. However, they offer poor water resistance and high cost, drawbacks that can be reduced when combined with acrylic polymers. Thus, the combination of polyurethanes and acrylic polymers (polyurethane/acrylic hybrid dispersions) results in coatings with superior properties [1,2].

Waterborne polyurethanes are mainly obtained by a step-growth polyaddition reaction taking advantage of the so-called acetone process [3,4]. In this process, the polyurethane is synthesised in acetone using an acid-functionalized diol, which acts as internal emulsifier. Afterwards, water is added to the reaction medium and nanoprecipitation of the polymer takes place. Lastly, the solvent is removed, and the Volatile Organic Compound (VOC) free waterborne polyurethane dispersion is obtained. However, acrylic latexes are produced by radical

chain emulsion polymerisation reaction [5]. This demonstrates that there are important differences between the processes for obtaining waterborne polyurethanes and acrylic emulsions, and most significantly, the blends of these polymers present poor properties because of the low compatibility between urethane and acrylic phases. Accordingly, several strategies have been employed to develop polyurethane/acrylic hybrids with good compatibility [6]. The simplest way to combine both polymers is to mix previously prepared polyurethane and acrylic dispersions. Nevertheless, since the compatibility between both components is low, the resulting dispersion exhibits phase separation. This challenge in terms of compatibility, could be overcome using different synthetic strategies. With this purpose, the waterborne polyurethane can be synthesised in a first step and, after the water addition, the acrylic polymer is in situ generated by radical polymerisation. Some authors add the acrylic monomer as solvent in the polyurethane synthesis reaction [7] while others add the acrylic monomer once the polyurethane dispersion
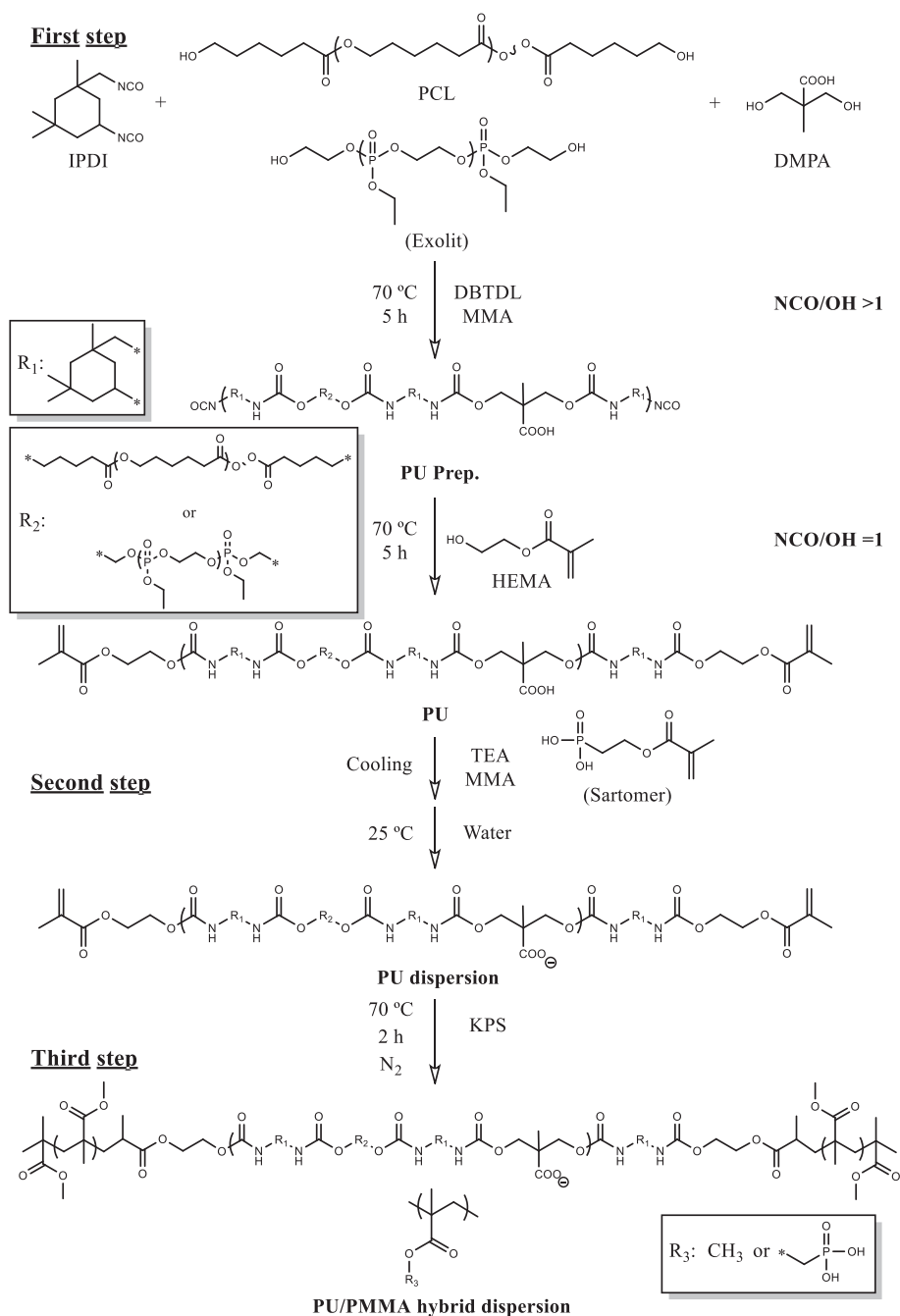
Scheme 1. Synthesis of the PU/PMMA dispersion.

is generated [8]. In terms of sustainability, the first method presents advantages, since no volatile organic compounds are used.

Regardless of the synthesis method, the polyurethane and acrylic phases are not completely compatible, and the final dispersion can present a biphasic morphology. In order to increase compatibility, acrylic moieties can be introduced into the polyurethane structure using hydroxyacrylates. These monomers are introduced as chain ends into the polyurethane structure and are able to covalently link both phases, increasing the compatibility and improving the properties of the final coating [9].

An especially important application of Polyurethane/acrylic hybrid dispersions is wood coating [10,11]. In this application, the coating must protect the substrate, but additionally the aesthetic properties of wood should be maintained. In order to fulfil this requirement, the coating must be transparent. In addition, due to the inherent

flammability of wood, there is a growing interest in the development of fire resistant coatings [12,13]. However, the addition of flame-retardant compounds often leads to a decrease in the transparency of the coating. The introduction of covalently bonded fire retardant has proven to be a good strategy to attain good flame-retardant properties while maintaining the transparency of the coating. Thus, several polyurethane (and acrylic latex) dispersions have been covalently modified with flame-retardant compounds [14–19]. However, reports on fire-retardant polyurethane/acrylic hybrids are scarcely found in open literature.

In light of the above, the present work deals with the preparation of phosphorous-modified polyurethane/acrylic hybrid dispersions for flame-retardant transparent wood coatings. The phosphorous compounds were covalently linked to both, polyurethane and acrylic phases, and the effect of phosphorus on dispersion characteristics and fire-retardant properties were analysed by thermogravimetry and pyrolysis

Table 1
Nomenclature and description of the different dispersions.

Samples	IPDI [g (mmol)]	PCL [g (mmol)]	DMPA [g (mmol)]	Exolit [g (mmol)]	MMA [g (mmol)]	Sartomer [g (mmol)]
PU/PMMA_w/o_HEMA	10.19 (45.85)	31.00 (15.50)	4.07 (30.35)	–	28.68 (286.46)	–
PU/PMMA_DMPA15%	10.19 (45.85)	30.69 (15.35)	4.07 (30.35)	–	28.68 (286.46)	–
PU/PMMA	13.56 (60.98)	30.69 (15.35)	6.10 (45.48)	–	28.68 (286.46)	–
PU/PMMA_E40%	13.56 (60.98)	18.41 (9.21)	6.10 (45.48)	4.05 (6.14)	28.68 (251.27)	–
PU/PMMA_E50%	13.56 (60.98)	15.35 (7.68)	6.10 (45.48)	5.06 (7.67)	28.68 (251.27)	–
PU/PMMA_E60%	13.56 (60.98)	12.28 (6.14)	6.10 (45.48)	6.08 (9.21)	28.68 (251.27)	–
PU/PMMA_E70%	13.56 (60.98)	9.21 (4.60)	6.10 (45.48)	7.09 (10.74)	28.68 (251.27)	–
PU/PMMA_S10%	13.56 (61.00)	30.69 (15.35)	6.10 (45.48)	–	25.81 (226.13)	2.87 (14.80)
PU/PMMA_S20%	13.56 (61.00)	30.69 (15.35)	6.10 (45.48)	–	22.95 (201.07)	5.73 (29.54)
PU/PMMA_E50%_S5%	13.56 (61.00)	15.35 (7.68)	6.10 (45.48)	5.06 (7.67)	27.25 (238.74)	1.43 (7.37)

combustion flow calorimetry. The best dispersions were tested as wood coatings.

2. Experimental

2.1. Materials

Isophorone diisocyanate (IPDI, Sigma-Aldrich; 98 %), poly-caprolactone diol (PCL, Sigma-Aldrich; Mn ∼ 2000 g·mol^{-1}), 2,2-bis (hydroxymethyl)propionic acid (DMPA, Sigma-Aldrich; 98 %), methyl methacrylate (MMA, Sigma-Aldrich; 99 %), dibutyltin dilaurate (DBTDL, Sigma-Aldrich; 95 %), 2-hydroxyethyl methacrylate (HEMA, Sigma-Aldrich; 97 %), triethylamine (TEA, Sigma-Aldrich; ≥99 %), potassium persulfate (KPS, Sigma-Aldrich; ≥99.0 %), deionized water (Quimibacter, <1 μS·cm^{-1}), polyethyl-phosphate glycol ester (commercially named as Exolit® OP 550, Clariant; 660 g·mol^{-1}, phosphorus content16–18 wt%), phosphate ester of 2-hydroxyethyl methacrylate (named as Sartomer® 9054, Arkema Group, phosphorus content 16 wt%), VOC-free silicone-containing defoamer for aqueous systems commonly named BYK 028 (BYK Chemie GmbH; VOC <1500 ppm), silicone surfactant for aqueous coatings known as BYK 346 (BYK Chemie GmbH; active ingredients 52 %), 2-butoxyethanol (BG, Dow Chemicals), and non-ionic polyurethane in butyl triglycol/water rheology modifier called Tafigel® PUR 60 (Müzing Chemie; active ingredients 40 %) were used as received.

2.2. Synthesis

PU/PMMA dispersions were prepared using three-steps (Scheme 1). This synthesis took place in a jacketed reactor attached to a water bath.

In the first step, the PU prepolymer was obtained by the reaction between the diisocyanate (IPDI) and the diol (PCL). MMA was used as solvent (60 % of the final MMA amount was added) and DBTDL (0.03 wt % of the PU) as catalyst. In this step, acid groups were incorporated by means of an internal emulsifier (DMPA) in order to obtain stable dispersions. The reaction was mechanically stirred at 200 rpm and continued at 70 °C for 5 h. HEMA was subsequently incorporated (0.040 g, 0.310 mmol) and left for further 5 h. At this point the NCO/OH ratio was 1, and the chains were end capped with acrylic moieties.

In the second step, water was added giving rise to a dispersion. For this, the reactor was cooled to 25 °C and afterwards TEA (TEA:DMPA molar ratio 1.05:1) and the remaining MMA (40 % of the final MMA amount) were placed. TEA neutralised the acid groups to obtain stable particles upon completion of the phase inversion to water. For this process, half of the final water quantity was added (addition rate 3 mL· min^{-1}). The total amount of water resulted in a final solids content of 24 wt%.

In the third step, the MMA of the particles was polymerised. Thus, the initiator (KPS) was added (0.05 wt% of the total MMA amount), and the reaction proceeded for 2 h at 70 °C under nitrogen atmosphere. The remaining water was incorporated after complete synthesis.

Table 2
Formulation of the wood coatings.

		F_PU/ PMMA	F_PU/ PMMA_E50%	F_PU/ PMMA_S10%
Dispersion	[wt %]	96.2	96.0	96.6
Defoamer	[wt %]	1.1	1.0	1.0
Coalescent	[wt %]	1.1	1.1	1.0
Thickener	[wt %]	0.5	0.8	0.5
Surface additive	[wt %]	1.1	1.2	1.0
Formulation solids content	[wt %]	24.6	24.6	24.5

In order to produce flame retardance, two different phosphorous compounds were incorporated. A diol phosphate, named Exolit OP 550, and a methacrylate phosphate, denoted Sartomer 9054. As Exolit replaced the PCL diol, it was incorporated at the first step to keep the NCO/OH ratio constant. Sartomer substituted the MMA and therefore it was incorporated once the PU was obtained (third step). Weight ratio of the PU and the acrylic part was maintained constant.

Table 1 summarises the synthesis reaction. The different dispersions obtained were named according to the changes made on the basis of the so-called PU/PMMA dispersion. Note that PU/PMMA_w/o_HEMA and PU/PMMA_DMPA15% referred to the dispersion obtained without and with HEMA capping the PU prepolymer, respectively. Both dispersions contained 15 wt% of DMPA of the total amount of PU. For all the other dispersions, the employed DMPA amount was increased to 20 wt%. The letter E stood for the diol phosphate Exolit and S for Sartomer. The following number indicated the weight percentage of the PCL or/and MMA that were replaced by Exolit or/and Sartomer, respectively.

2.3. Coating preparation

Wood coatings were formulated mixing some of the dispersions with a VOC-free defoamer (BYK 028), a coalescent agent (BG), a thickener (Tafigel® PUR 60) and silicon surface additive (BYK 346) as shown in Table 2. All components were mechanically stirred at 10^4 rpm for 10 min in a DISPERMAT CV3 Plus from VMA-GETZMANN GmbH dissolver. Different components were added, and their concentration was adjusted in order to obtain good film formation properties.

2.4. Measurements

2.4.1. Neat polyurethane/acrylic hybrids

Infrared spectra were recorded in a Nicolet 6700-IR (Thermo Scientific) in ATR mode (Specac MKII Golden Gate). Experiments were performed using 10 scans and a resolution of 4 cm^{-1}.

Dry films were dissolved in deuterated chloroform and ^{1}H NMR

experiments were performed in a Bruker (Advance 300 DPX model).

The coatings of neat polyurethane/acrylic hybrids were obtained after casting the dispersions described in Table 1 on Teflon moulds for 3 days at room temperature and other 3 days under vacuum. These samples were used for DSC, TGA, NMR, gel content and microcalorimetry experiments. For contact angle measurements, samples were cast over glass microscope slides using a 100 μm applicator and were dried in the same way as described before.

The average molar masses of the synthesised dispersions were determined in a Thermo Scientific size exclusion chromatograph (SEC), containing a refractive index detector (RefractoMax 521) and an isocratic pump (Dionex UltiMate 3000). Measurements were performed in Tetrahydrofuran (THF) at a flow rate of 1 mL·min^{-1} and polystyrene calibration standards ranging from 162 g·mol^{-1} to 3,150,000 g·mol^{-1} were used. The measurements were carried out at 25 °C. Dry samples were dissolved in THF at a final concentration of approximately 2.8 wt% and filtered before injection.

The absolute molar mass distribution of the polymer was measured by Asymmetric-Flow Field-Flow Fractionation (AF4) in combination with a multi-angle light scattering (MALS) Dawn Heleos II (Wyatt Technology) and a refractive index (RI) detector Optilab Rex (Wyatt Technology). THF was used as the mobile phase and fractionation was controlled by a Wyatt Eclipse 3 AF4 separation system controller. The spacer used in the channel was 490 μm width and the membrane was of regenerated cellulose with a cut-off 10 KDa. The samples were prepared at about 10 mg polymer ·mL^{-1} THF and 100 μL of solution were injected without prior filtration. The data collection and treatment were carried out by ASTRA software version 6.1 (Wyatt Technology). The absolute molar mass was calculated from the MALS/RI data using the Debye plot with first-order Zimm and second-order Berry formalism. For the specific refractive index increment value (dn·dc^{-1}), the average of the PU (60 wt%, dn·dc^{-1} = 0.149 mL·g^{-1}) and MMA (40 wt%, dn·dc^{-1} = 0.084 mL·g^{-1}) were considered. Therefore, the employed dn·dc^{-1} value was 0.123 mL·g^{-1} and the measurements were carried out at room temperature.

Particle size was analysed by dynamic light scattering (DLS) (90Plus Particle Size Analyzer, Brookhaven Instruments). Measurements were conducted at a fixed angle of 90°, and at temperature of 25 °C. A refractive index of 1.520 was employed. Before the measurement 50 μL of the dispersion were diluted with 1.5 mL of distilled water.

Transition electron microscopy (TEM) was employed to analyse the morphology of the final particles in a Talos F200i (Thermo Scientific) field emission gun instrument equipped with Bruker XFlash 100 XEDS spectrometer. Images were performed in the STEM mode under high annular dark field (HAADF) detector for Z contrast imaging in STEM conditions. Those conditions were a camera length of 160 mm and a semiconvergent angle of 6 mrad. The dispersions were diluted is distilled water (0.05 wt%) and sonicated for 1 h before letting them dry at ambient temperature over standard TEM copper grids (200 Mesh) covered by a pure carbon film. The grid was glow discharged before the drop of suspension was added.

The gel content of the dry coatings was determined by Soxhlet extraction in THF. Samples of about 1 g were placed on the corresponding filter paper bags, and they were dried for 24 h at 60 °C. Then, the extraction was left for 24 h. Finally, samples were left to dry for another 24 h at 60 °C. The results were the average of three measurements.

Water static contact angle (CA) was determined using the sessile drop method in a Phoenix 300 (Surface Electro Optics) goniometer with an image processing system (Data Physics Instruments GmbH). A drop size of about 20–50 μL was employed and the average value was calculated from at least eight readings.

Differential scanning calorimetry (DSC) measurements of the dried samples were performed on a TA Instruments DSC Q2000. Samples were heated in nitrogen from −80 °C to 150 °C at a heating rate of 10 °C·min^{-1}. A second run was done using the previous conditions after

cooling the samples at 50 °C·min^{-1}. About 3–5 mg of the sample were used for each analysis.

Thermogravimetric analyses (TGA) were performed on a TGA Q500 from TA Instruments. Dry samples were heated under nitrogen from 30 °C to 800 °C using a heating rate of 10 °C·min^{-1} and under a nitrogen flow of 90 mL·min^{-1}. About 5–25 mg of the sample obtained by casting were used for the analyses.

Flammability of the coatings was determined in a pyrolysis combustion flow calorimetry (PCFC) from Fire Testing Technology. 6–8 mg of samples were heated at a rate of 1 °C·s^{-1}. The sample was heated to 700 °C, and a combined gas flow rate of 100 mL·min^{-1} (oxygen concentration of 20 vol%) was applied in the combustor (temperature 900 °C). A total of three measurements were performed for each sample. The heat release capacity (HRC), peak release rate (pHRR) and total heat release rate (tHRR) were calculated from the oxygen consumption, heating rate, sample weight and flow rate.

A gas chromatograph (Shimadzu GC 14-A with a SGE BP-624 column) was employed to determine the MMA amount in the final dispersion. The measurements were carried out at a 170 °C injector temperature, 250 °C detector temperature, under helium gas and under a constant pressure of 0.5 kg·cm^{-2}. The employed temperature program was the following: 50 °C for 2 min, heated to 80 °C at a heating rate of 10 °C·min^{-1}, 80 °C for 5 min, heated to 100 °C at a heating rate of 5 °C·min^{-1}, 100 °C for 5 min, heated to 240 °C at a heating rate of 25 °C·min^{-1} and 240 °C for 3 min. For sample preparation 2 mg·g^{-1} of external standard pentanol and 5 mg·g^{-1} of a radical inhibitor (hydroquinone) were introduced into a 5 mL vial with 2 g of dispersion. 5 μL were injected.

2.4.2. Formulated coatings

Colorimetric measurements of the formulated wood coatings were carried out to quantify the film transparency using a CM-2600d Spectrophotometer (Konica Minolta). The CIELAB system values were determined by this technique: L* (lightness), a* (red and green) and b* (yellow and blue). L* values were analysed where zero represents black and 100 represents white. To consider the sample as transparent, values below 25–30 were those being sought. The given values were the average of at least 10 measurements.

The gloss of the different formulated coatings was determined in a glossmeter (BYK GARDNER micro-TRI-gloss) according to UNE-EN ISO 2813:2014. For this purpose, the light reflected by the surface at different incidence angles was measured, being 20° for highly reflective surfaces, 60° for semi-gloss surfaces and 85° for matte surfaces respectively. Initially, all samples were analysed at 60° and if the result obtained was <10 gloss units, it was considered a matte surface and the analysis was repeated at the corresponding geometry. In contrast, if the value obtained exceeded the 70 gloss units, it was deemed a highly reflective surface and a geometry of 20° was required to obtain the real result. A mean value of 10 measurements was reported. For this purpose, formulations were applied on dark glass using a 120 μm thick Baker Applicator (Neurtek Instruments). Furthermore, sapele and oak wood substrates were employed, for which three light layers of about 80 g·m^{-2} each were applied. The samples were dried for a week at room temperature prior to analysis.

Adhesion to the different substrates of the formulated coatings was measured using a cross-cut tester following the UNE-EN ISO 2409:2020 standard. The wood substrates chosen were sapele and oak thus, the incisions were made with 2 mm spacing, using a 9 mm width edge cutter (NT-cutter, Zehntner GmbH Testing Instruments) and a ZCT 2160.2 Cross-cut Template (Zehntner GmbH Testing Instruments) and a roll 25 mm width adhesive tape (Zehntner GmbH Testing Instruments) was also necessary to complete the test. For sample preparation the same procedure as for gloss measurement was followed but just wood substrates were analysed.

The water resistance of the formulated coatings was determined using an internal procedure. A small cotton amount was wetted with
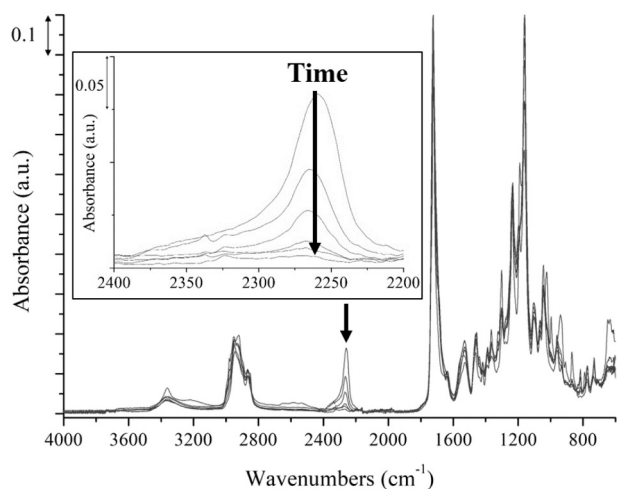
Fig. 1. FTIR of the PU/PMMA sample at different PU polymerisation reaction times.

about 2 mL of water and then placed on top of the sample and covered with a watch glass. The water was left for 3 h, and the changes were noted.

In terms of transparency and water sensibility, the formulations were

applied on contrast white/black cardboards (B/N test charts from Neurtek Instruments) using an ATX Automatic Applicator (Neurtek Instruments) at a 40 mm·min^{-1} application rate and a 120 μm thick Baker Applicator (Neurtek Instruments). Prior to the measurements, samples were dried for one week at room temperature.

A Fisher Instruments ultramicrohardness device (Fischerscope® H100) with a Vicker indenter was used to compare the hardness of the formulated films. The test proceeded by loading and unloading cycles in the range of 0.4–10 nN. Each cycle was divided into 40 loading steps with an intermediate time of 0.5 s, resulting in a total loading time of 19.5 s. A mean value of five measurements was registered. The analysis was performer on the same dark glass samples as gloss and the films were left to dry for at least 2 weeks under ambient conditions, ensuring that the films were completely dried.

Cone calorimetry tests were done in order to analyse the fire reaction performance of the samples. For this purpose, time to ignition (TTI), total heat release rate (THR), effective heat of combustion (EHC), peak heat release rate (pHRR), time to peak heat release rate (TT pHRR), final residue and released CO and CO_2 were analysed according to ISO 5660-1:2015. An incident heat flux of 50 kW·m^{-2} was applied at a distance of 25 mm from the heater and the tests were executed in a horizontal orientation. In order to carry out the measurements, the dispersions were applied to 88.4 mm surface area substrates (Fimapan, wooden particle boards from FINSA) and the final thickness obtained was about 12 mm. 3 g of the final formulation were applied and left dry for 24 h at 20 °C and after the second application of 3 g and drying for another 24 h
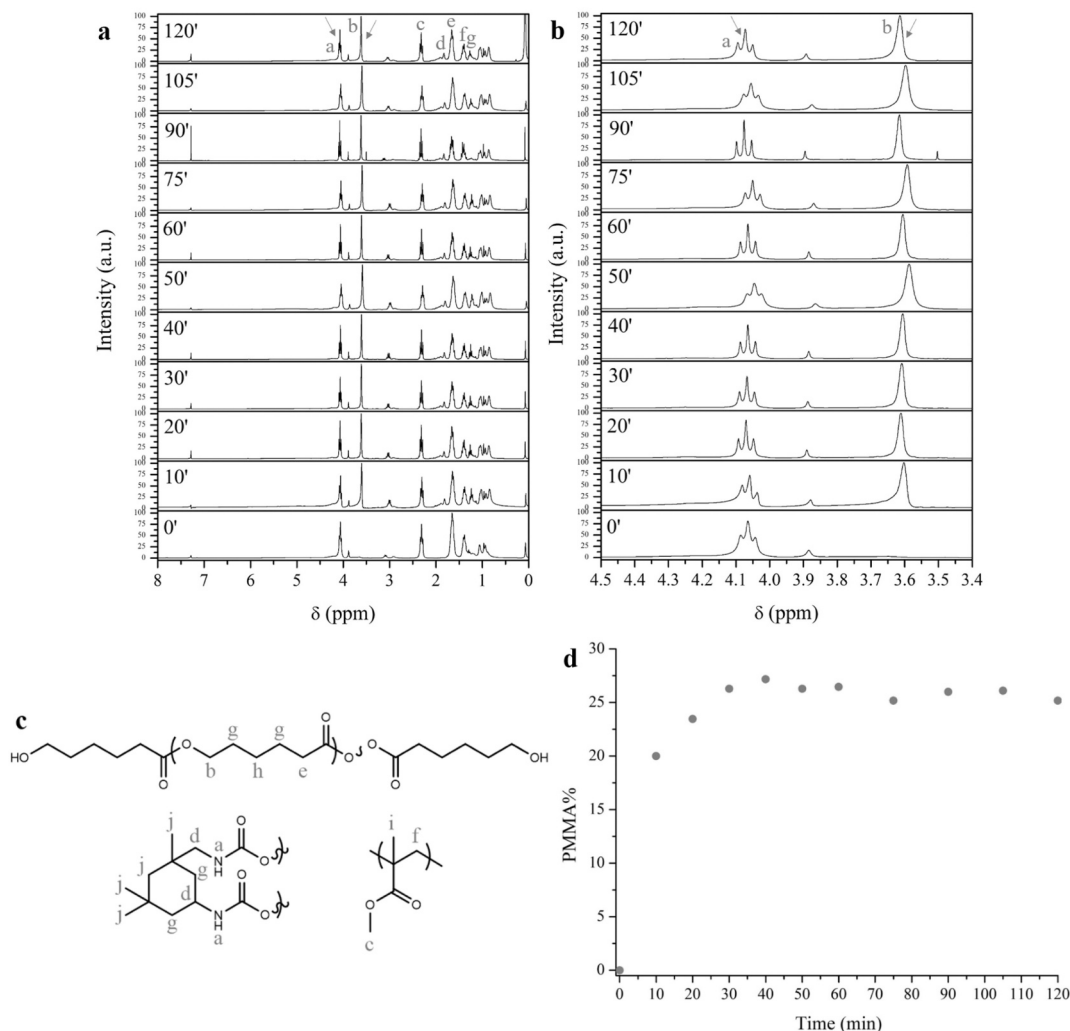

Fig. 2. a) ^{1}H NMR of the dispersion PU/PMMA_w/o_HEMA with time b) Magnification of the spectra, c) Structure and d) PMMA wt% versus time.
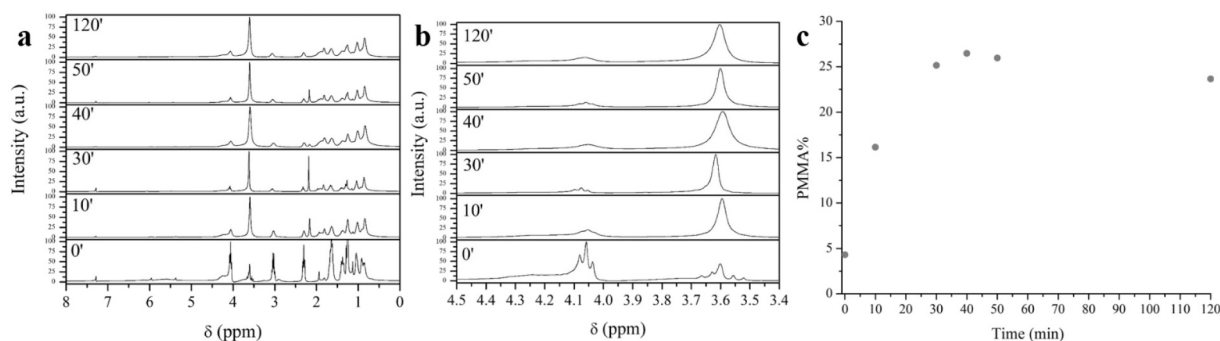
Fig. 3. a) ^{1}H NMR of the dispersion PU/PMMA_E50% with time, b) Magnification of the spectra and c) PMMA wt% versus time.

at 37 °C, they were left in the conditioning room (50 % relative humidity and 23 °C) for 3 days. The measurements were reproducible within ±10 %, thus the data reported were the average of two replicates.

3. Results and discussions

3.1. Synthesis and chemical characterization of the PU/acrylic hybrid. FTIR/NMR/SEC/AF4/STEM

FTIR and NMR were employed to follow the PU synthesis reaction and the MMA polymerisation, respectively.

The PU reaction, as explained in previous section, took place in two steps: first, an NCO end capped prepolymer was obtained (5 h) and afterwards, HEMA was added to complete the reaction. The first step of the reaction was followed by infrared spectroscopy as it is very appropriate to monitor the isocyanate disappearance. The infrared spectra were recorded at different reaction times after drying the samples in order to evaporate the MMA. The spectra for the first reaction are shown in Fig. 1. As expected, the absorbance of the isocyanate characteristic stretching band at 2260 cm^{-1} decreased throughout the reaction. In addition, the generated urethane groups were responsible for the bands at 3325 cm^{-1}, 1710 cm^{-1} (amide I) and 1533 cm^{-1} (amide II) (corresponding to the stretching vibration of –NH and -C=O and bending vibration of –NH, successively) [3,20]. All these changes confirmed the formation of urethane groups. Moreover, after 5 h, the absorbance of the isocyanate stretching was negligible, corroborating that the first step was successfully completed.

Likewise, the same procedure was followed when Exolit was incorporated into the polymer chain. Infrared spectra for PU/PMMA_E50% sample are shown in Fig. S1. The disappearance of the isocyanate stretching vibration after 5 h confirmed the introduction of the phosphorylated polyol in the polymer structure.

In order to follow and quantify the PMMA/urethane ratio during the reaction ^{1}H NMR was employed. The spectra obtained for the PU/PMMA_w/o_HEMA dispersion are shown in Fig. 2a and its scale-expanded spectra in Fig. 2b. The main signals corresponded to IPDI, PCL and PMMA as can be appreciated in the signal assignment displayed in Fig. 2c. Note that the spectra were recorded after removal of the

unpolymerised methyl methacrylate, so that the monomers characteristic double bond signals between 5 and 6 ppm were not visible in any spectrum. The area at 3.60 ppm (corresponding to the poly(methyl methacrylate) methyl nuclei attached to the oxygen side of the ester) was quantified taking as reference the signal at 4.15 ppm (concerning to the methylene nuclei of PCL attached to the ester group) (see Fig. 2c). The PMMA weight percent of the hybrid dispersion is shown in Fig. 2d [21].

Based on the results obtained, it is worth noting that the poly(methyl methacrylate) percentage reached a maximum in 40 min and afterwards remained constant suggesting that there was no methyl methacrylate monomer available to react. The final PMMA percentage was close to 30 % even though according to the reaction stoichiometry a theoretical value of 40 wt% should be reached. In order to establish the origin of these differences, the residual monomer concentration was measured by GC and a value of 500 ppm was obtained. Even though this value was high, the residual monomer could not explain the reduction of the PMMA content in the polymer. For the purpose of ensuring that there was no more MMA available to react, an excess amount of thermal initiator was incorporated and made to react for another 2 h. The NMR spectrum obtained are shown in Fig. S2 and as can be seen there was no change on the PMMA signal area. Therefore, we argued that the rest of the methyl methacrylate was evaporated during the synthesis because of a non-appropriate sealing of the reactor.

Similarly, the polymerisation of the MMA was also studied for the sample containing Exolit (Fig. 3) and the results were similar to the previous ones. On the one hand, as in the non-phosphorus containing hybrid, the PMMA percentage reached the maximum in 40 min. On the other hand, the PMMA content was lower than the theoretical one which was related to the evaporation of the monomer (residual monomer content of the sample was 50 ppm). In light of the above, it was clear the Exolit had not significant effect on the MMA polymerisation rate.

The incorporation of the acrylic phosphate Sartomer to the polymer could not be followed by ^{1}H NMR because there were no isolated signals for this monomer. However, the incorporation of this monomer could be corroborated by FTIR (Fig. S3). As observed, pure Sartomer presented a strong absorption in the 900–1000 cm^{-1} region that was related to the phosphate stretching vibration. This signal was present on sample PU/PMMA_S10%. Moreover, no band assigned to the C=C stretching was observed corroborating the polymerisation of the double bond and the successful incorporation of Sartomer in the resin.

It is to mention that the reactions gelled in the first step when >70 % of the polyol was replaced by phosphorylated polyol. Similarly, gelation occurred in the third step when >10 % of MMA was replaced by the phosphorylated acrylate or when both phosphorylated compounds were added. The gelation of the reaction in the first step could be related to the phosphate ester exchange reaction. According to the literature, phosphate esters (such as Exolit) can produce transesterification reactions with alcohols [22]. It could be argued that the occurrence of the reaction between Exolit and the polyol produced cross-linking points and therefore it was in the origin of the gelation. Furthermore, the

Table 3
Gel content and molar masses measured by SEC/RI.

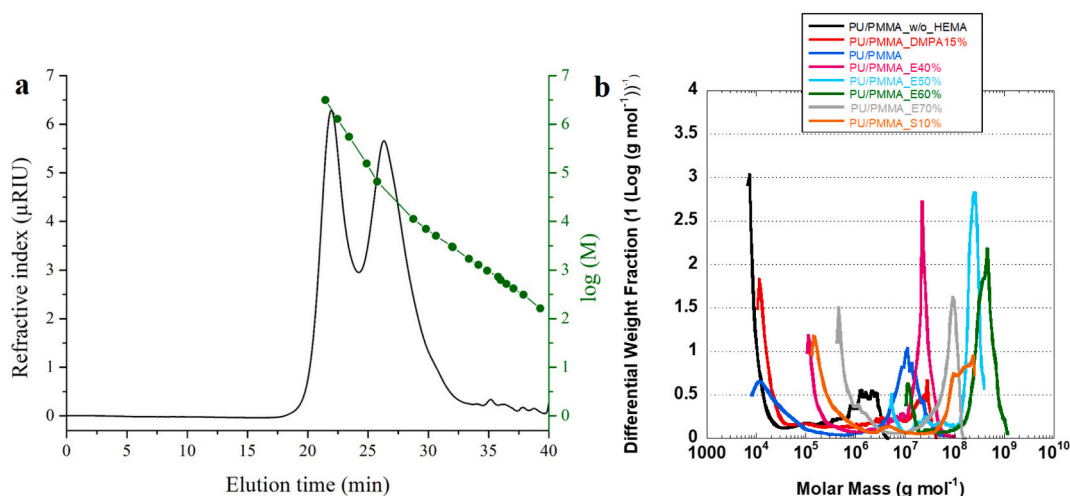|	$\overline{M_n}$ [g·mol^{-1}]	$\overline{M_w}$ [g·mol^{-1}]	Đ	Gel [%]
PU/PMMA_w/o_HEMA	21,706	46,372	2.1	0
PU/PMMA_DMPA15%	21,593	56,855	2.6	0
PU/PMMA	18,435	49,599	2.7	0
PU/PMMA_E40%	11,368	41,636	3.66	65 ± 11
PU/PMMA_E50%	12,410	33,067	2.66	53 ± 1
PU/PMMA_E60%	8594	13,822	1.61	41 ± 36
PU/PMMA_E70%	9650	17,934	1.86	30 ± 6
PU/PMMA_S10%	7356	17,373	2.36	66 ± 2

Fig. 4. a) PU/PMMA sample SEC chromatogram and b) molar mass distributions obtained by AF4/MALS/RI for different hybrids.

gelation produced with the addition of Sartomer, was related to the phosphoric acid groups that aggregated and cross-linked during the polymerisation [20].

As a consequence of the gelation, the maximum phosphorus amount that could be incorporated in the polymers (calculated considering the phosphorus content of Exolit and Sartomer provided by the manufacturer) was limited to 1.73 ± 0.14 wt%. Moreover, the introduction of phosphorus in the formulation promoted the above-mentioned cross-linking reactions and the dried films presented high values of the gel content (Table 3). Surprisingly, the gel content decreased with the Exolit amount. The origin of this unexpected result was related to the phosphate ester interchange reaction. As stated previously, this reaction provoked the formation of crosslinking points and therefore it was not possible to use high Exolit amount. However, because of the structure of the phosphorylated polyol, the interchange reaction could also give rise to formation of monofunctional alcohols, which could act as chain stoppers reducing the molecular weight. Consequently, it seems that with increasing the Exolit concentration the gel content was reduced because of the chain stopper effect. However, there was a concentration where the crosslinking effect became predominant and the reaction gelled. Finally, the highest gel content was reached for the Sartomer containing sample. Accordingly, the cross-linking ability of the phosphorous acrylate was higher than that of the phosphorous containing polyol.

SEC/RI was used to determine the molar mass of polymers. Fig. 4a

shows the SEC chromatogram of the PU/PMMA sample. Most significantly, a bimodal distribution was observed. This distribution was a consequence of the different molar mass of the polyurethane and acrylic chains. As the poly(methyl methacrylate) was obtained by radical polymerisation, it could be argued that it was responsible for the high molar mass fractions. It is worth noting that this signal appeared at the exclusion limit of the employed SEC column. Therefore, only the polyurethane fraction was characterized by SEC/RI (Table 3).

As observed in Table 3, among the samples without phosphorous, the molar mass (Mw) and polydispersity index of the polyurethane was slightly higher for the samples compatibilized with HEMA. As HEMA was located as chain end in the Polyurethane backbone, it could be polymerised by radical polymerisation and therefore this effect increased the molecular weight. The samples containing phosphorous were filtered before injection in SEC/RI due to the high gel contents arising from the cross-linking reactions. Therefore, only the soluble part was analysed. However, with the addition of the phosphorous compounds, the molar mass of the polyurethane chains decreased considerably. This result was related to the interchange reaction that could gave rise to formation of monofunctional alcohols, reducing the molecular weight of the Polyurethane as well as the gel content, as stated previously.

With regard to the data obtained by AF4/MALS/RI (Fig. 4b), a bimodal molar mass distribution was observed for all the hybrid polymers as well as the SEC/RI results. The hybrid without acrylic
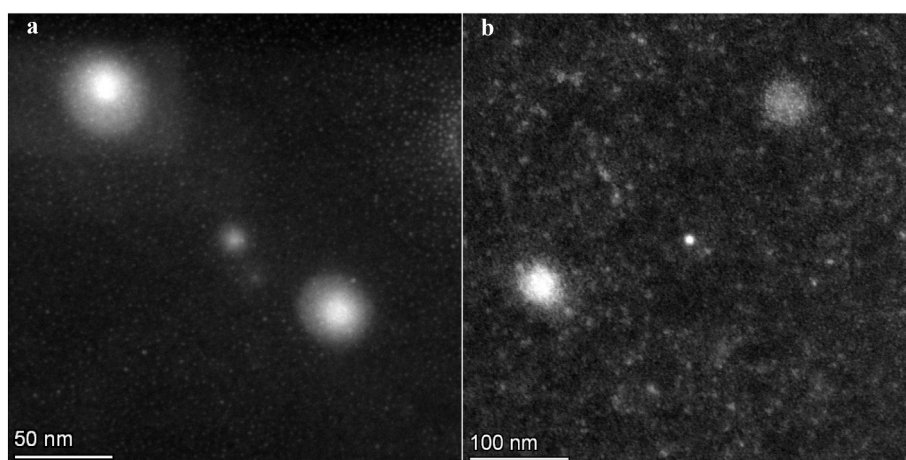

Fig. 5. STEM analysis of the sample PU/PMMA. At a scale bar of a) 50 nm and b) 100 nm.
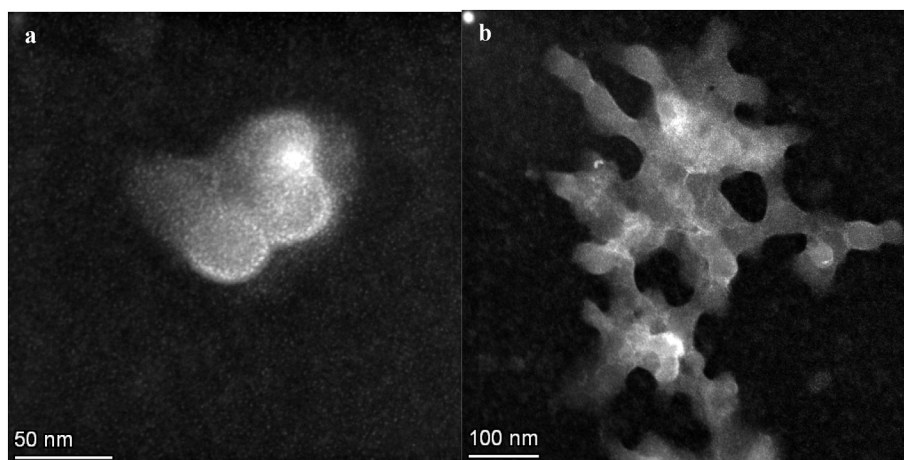
Fig. 6. STEM analysis of the sample PU/PMMA_E50%. At a scale bar of a) 50 nm and b) 100 nm.
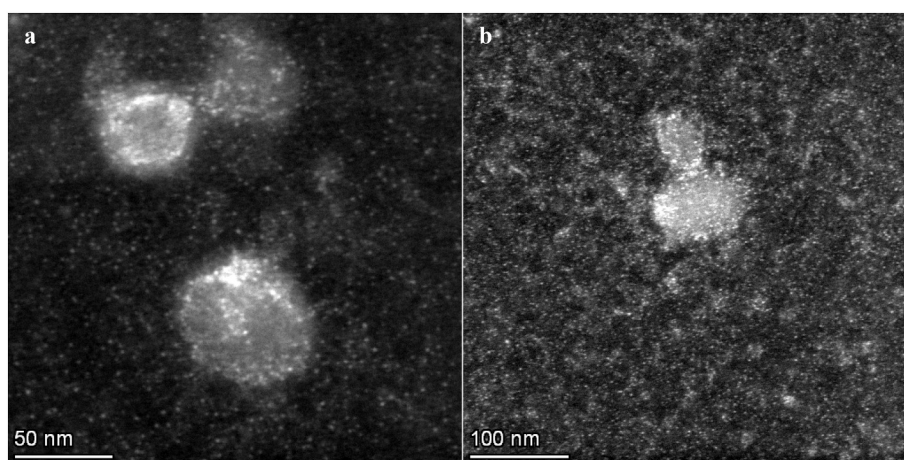

Fig. 7. STEM analysis of the sample PU/PMMA_S10%. At a scale bar of a) 50 nm and b) 100 nm.

compatibiliser (PU/PMMA_w/o_HEMA) showed a low molar mass peak at about 10^4 g·mol^{-1} which agreed with the molar mass observed in the SEC/RI for the polyurethane fraction (Table 3) and another peak at higher molar masses (10^6 g·mol^{-1}) corresponding to the acrylic fraction. These values were very close to those reported in literature for similar hybrids [23]. However, the incorporation of HEMA (sample PU/PMMA_DMPA15%) caused a shift to higher molar masses in both peaks.

Even though all the hybrids that did not contain phosphorous presented considerably high molar masses, they did not present any gel. On the contrary, when the phosphorous compounds (Exolit/Sartomer) were used, as mentioned, significant gel content values were obtained (Table 3). AF4/MALS/RI offered the possibility to analyse the whole sample (including gel). Thus, when the Exolit containing samples

(without filtration) were analysed by AF4/MALS/RI both peaks shifted to higher molar masses comparing to the no phosphorylated samples. Opposite results were registered for the Polyurethane fraction by SEC-RI, probably because of the difficulty of AF4/MALS/RI in measuring the low molar masses when very high molar masses (gel) are present. However, it was not observed a clear trend between the molar mass and the Exolit content but the measured huge molar masses should be related with the grafting and cross-linking generated by the transesterification side reaction. In relation to the addition of Sartomer, the increase of the molar mass of both segments was a consequence of the high interactions between the phosphoric acid groups and chemical cross-linking reactions [24].

The morphology of the particles was studied by STEM images. The results are shown in Figs. 5, 6 and 7, for dispersions PU/PMMA, PU/PMMA_E50% and PU/PMMA_S10% respectively. This technique is able to detect different electronic densities; therefore, it can be useful to elucidate the distribution of the PU and PMMA in the particles. Different types of particles of diameter close to 50 nm were appreciated in the sample PU/PMMA. Some showed higher contrast than others. According to the literature, the high contrast particles contained high PMMA amount while the low contrast ones contained high PU percentage [10,25]. Some core-shell morphology particles could be distinguished here and there where the PU surrounded the PMMA core [25] [10].

On the other hand, it was observed that the incorporation of Exolit (Fig. 6) caused coalescence of the particles to such an extent that it created cross-linked structures. The incorporation of Sartomer (Fig. 7),

Table 4
Properties of the dispersions and films.

Samples	Particle size [nm]	Water contact angle [°]
PU/PMMA_w/o_HEMA	49 ± 1	78 ± 3
PU/PMMA_DMPA15%	72 ± 1	79 ± 1
PU/PMMA	55 ± 1	77 ± 2
PU/PMMA_E40%	90 ± 2	83 ± 3
PU/PMMA_E50%	82 ± 1	71 ± 1
PU/PMMA_E60%	259 ± 4	62 ± 2
PU/PMMA_E70%	302 ± 73	55 ± 2
PU/PMMA_S10%	116 ± 8	79 ± 3

Fig. 8. DSC first heating run.

Table 5
Data obtained from TGA results.

Samples	P[a] [wt%]	T_{onset}[b] [°C]	T_{max}[c] [°C]	Residue at 800 °C in N_2 [%]
PU/PMMA_w/o_HEMA	–	212	333; 434	0.7
PU/PMMA	–	217	342; 404; 433	0.4
PU/PMMA_E50%	1.17 ± 0.10	191	309; 401; 427	2.1
PU/PMMA_S10%	0.55	185	329; 407; 435	0.2

[a] P: theoretical phosphorus content.
[b] T_{onset}: Temperature at which the weight loss was 5 % of the total mass.
[c] T_{max}: Temperature at maximum weight loss rate calculated from DTG.
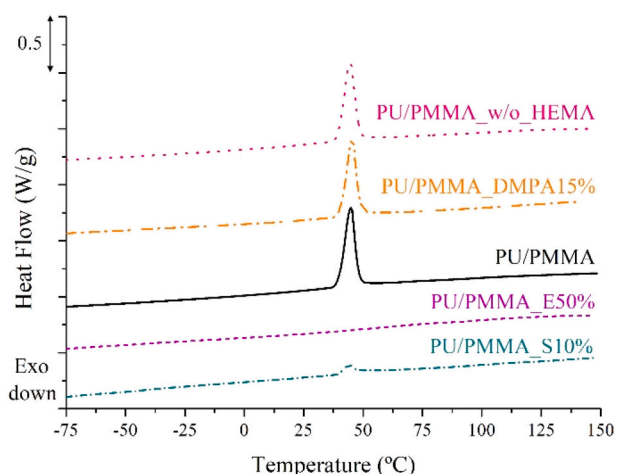
in contrast, gave a lower contrast matrix where high contrast particles could be observed. Thus, it could be said that a completely cross-linked PU film was obtained, where PMMA particles were dispersed.

3.2. Characterization of the dispersions

The main characteristic considered to optimise the dispersion was the particle size, since this is directly related to the final film appearance. Thus, considering that the final application of the synthesised dispersion was for wood coating, the film was intended to be transparent and consequently small particle size was required [26,27]. The obtained particles sizes are collected in Table 4.

The sample without HEMA presented a particle size close to 50 nm. It should be mentioned that the addition of a compatibiliser should make the films more transparent because it caused better component mixing [28]. However, the incorporation of the compatibilising agent increased the particle size from 49 to 72 nm. The particle size depended on the DMPA concentration and its location in the particle surface. Most probably, the chemical linkage between the phases reduced the mobility of the carboxylate groups toward the particle surface. Consequently, the particle size was higher for the HEMA containing samples. With the aim of maintaining a small particle size, as proposed by S.J. Peng et al. the amount of the internal emulsifier (DMPA) was increased [29,30] from 15 (PU/PMMA_DMPA15%) to 20 wt% (PU/PMMA), thus achieving a particle size close to 50 nm. It is worth noting that this data were in accordance with the STEM analysis.

Of a particular note, increasing the phosphorous compound concentration made the particle size increase and at this point, the film was no longer transparent. This effect was magnified when more Exolit was incorporated as the dispersions coagulated and could be related to both: a) the crosslinking of the polymer and b) the hydrophilic segments of Exolit since according to the literature more hydrophilic alcohols produce bigger particles [9].

The data obtained for the contact angle are summarised in Table 4. The results show that there were no important changes on the hydrophobic/hydrophilic character of the film with the addition of the compatibilising agent and the incorporation of a higher proportion of internal emulsifying agent. However, the introduction of the phosphorylated polyol reduced the contact angle, especially when the content was higher than 50, making the sample more hydrophilic. This result could be related to the polar groups of the phosphorous compounds that make the polymer more hydrophilic [31,32]. In addition, the phosphorylated polyol contained polyethylene oxide segments that could decrease the contact angle value. On the contrary, the contact angle was not modified by the introduction of the phosphorus containing acrylate, probably because of the low phosphorus content of the

dispersion.

3.3. Properties of the films

3.3.1. Pure resin

Pure resin dispersions were casted over microscope glass slides, and the photographs of the films can be found in Fig. S4. The film transparency was related to the PCL crystallisation as will be analysed in the following paragraphs.

Fig. 8 shows the DSC results and the data obtained from such analyses are summarised in the Table S1. In the first run, the samples that did not contain phosphorus showed a melting endotherm close to 50 °C which according to the literature corresponded to the crystalline PCL segments [33]. This transition was not present in the samples containing Exolit and Sartomer. In the second run all the samples were amorphous and presented two glass transitions. Therefore, as stated in literature, polyurethane and poly(methyl methacrylate) segments were phase separated. The low temperature transition (close to −50 °C) corresponded to the PU soft segment [34] while the transition near 100 °C was related to the PMMA part of the hybrid [35] and was probably overlapped with that of the PU hard segments.

As observed, for non-phosphorus containing samples, the introduction of the compatibilising agent did not produce significant changes in the PCL melting. However, in the second run the glass transitions of polyurethane and acrylic segments in sample PU/PMMA_DMPA15% were slightly closer from each other, suggesting once again that the HEMA acted as compatibilising agent. Moreover, with the increment of the DMPA from 15 to 20 wt% the high temperature glass transition showed superior values since the hard segment content was enlarged with the DMPA [36].

The introduction of phosphorous compounds produced an important decrease of the crystallinity of the PCL since the cross-linking restricted the PCL movement [37]. The decrease was even higher when Exolit was used due to the alteration of the chain regularity and the polyurethane packing provoked by the presence of a second diol [38]. There were no appreciable changes in the T_g when dealing with Exolit, whereas in the case of Sartomer, the PMMA T_g was increased. This could be explained by the high cross-linked structure of the samples containing Sartomer.

The TGA results obtained for the samples PU/PMMA_w/o_HEMA, PU/PMMA, PU/PMMA_E50% and PU/PMMA_S10% are summarised in Table 5 and the complete data obtained is shown in Fig. S5. The weight loss changes are more clearly observed in the differential thermogravimetry (DTG) curves. According to the literature, for PU/PMMA_w/o_HEMA two different weight loss steps could be distinguished: the first one corresponds to the decomposition of the hard segments and the second one to the soft segments and the acrylic part. By contrast PU/PMMA exhibited three stages instead of two, the one in the middle corresponding to the overlap of the soft segments and acrylic part [39]. Therefore, it would be concluded that the compatibilisation was
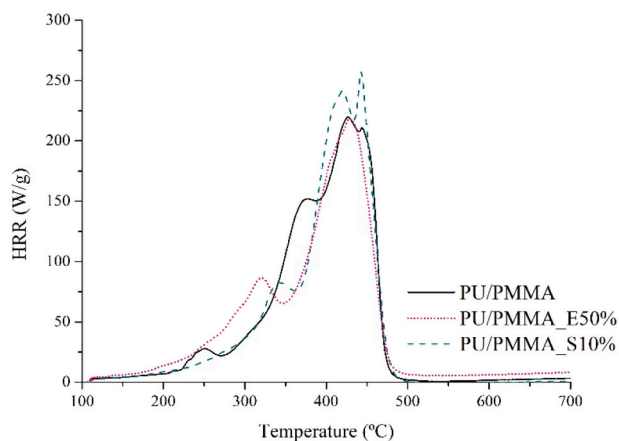
Fig. 9. Heat release rate against temperature obtained for different phosphorus content dispersions measured by microcalorimetry.

Table 6
Microcalorimetry data obtained for different formulations.

Samples	P [wt%]	HRC [J·g⁻¹· K⁻¹]	tHR [kJ·g⁻¹]	Residue at 700 °C in O₂ [%]
PU/PMMA	–	222 ± 5.5	24 ± 0.1	1.6 ± 0.4
PU/ PMMA_E50%	1.17 ± 0.10	226 ± 14.8	22 ± 0.6	2.5 ± 0.7
PU/ PMMA_S10%	0.55	268 ± 13.0	23 ± 0.3	1.5 ± 0.1

successful in some degree. These results were in accordance with those obtained by STEM and SEC.

Samples containing phosphorus showed a similar behaviour and the degradation took place in three steps. However, a remarkable change occurred in the onset degradation temperature, which decreased with the incorporation of phosphorus in the formulation. Therefore, it could be argued that the incorporation of the phosphorous compounds might accelerate the thermal decomposition of the matrix. According to the literature, phosphorus is considered to be the first element being released because P—O bond is weaker than the C—O one. The C—O bond requires of 256 kJ·mol⁻¹ whereas the P—O bond needs just 149 kJ· mol⁻¹ [19,38].

The released phosphorus remaining in the condensed-phase can promote the creation of a stable phosphorus-carbon layer at the surface and, thus, improve the thermal stability at high temperature [40]. Moreover, the phosphoric acid arising from the P—O decomposition could act as a urethane debonding catalyst and contribute to the polyol dehydrogenation, thereby decreasing the remaining steps temperatures as shown in the Fig. S5 data. Even though the incorporation of phosphorous compounds decreased the polymer degradation temperatures, it also could accelerate the formation of the char yield at high temperatures [38]. This could be the reason why when Exolit was used a slightly higher residue was obtained. However, due to the small phosphorus amount of the sample, the value of the residue was still low. It should be noted that for Sartomer there was no appreciable increase in the residual percentage. One reason for this could be that there was no enough phosphorus in the film to create the char [41].

Likewise, the result obtained for PU/PMMA, PU/PMMA_E50% and PU/PMMA_S10% by the microcalorimetry are shown in Fig. 9 and the data for HRC (heat release capacity), pHRR (peak heat release rate), tHR (total heat release), percentage of residue obtained and P (theoretical phosphorus weight percentage of the sample) are given in Table 6. As microcalorimetry involves analysing such small samples, the quantitative data obtained were not representative [42]. However, the data were

used to make a screening of the fire behaviour of all the formulations, and similar conclusions to those of the TGA were obtained. It was found that the first stage was related to the phosphorous compounds, which led to small heat release. Once the phosphorus was released, the phosphoric acid should generate the polymer dehydrogenation giving rise to a carbonaceous char. This layer should reduce the heat, O₂ and flammable gases transfer between the combustion and the non-combustion zones [43]. However, in the microcalorimetry the sample degradation takes place in the pyrolysis chamber, and not in real fire conditions. Thus, the released compounds are combusted at 900 °C. This could explain why there was only a small reduction in the total heat release. As regards the final residue data, similar results as for the TGA were obtained. The differences in these values were very small and may be due to the temperature at which they were measured and the use of the oxidative environment in the case of PCFCs.

3.3.2. Formulated dispersions

The transparency of the coatings was evaluated by colorimetric test (Table S2). The CIE L*a*b* colour system, also known as CIELAB, makes possible to quantitatively determine the colour of an object by means of three-dimensional Cartesian coordinates: L* (lightness), a* (red-green chromatic coordinate) and b* (yellow blue chromatic coordinate). This system is based on the statement that human cannot perceive red and green, yellow and blue or white and black at the same time. [44,45]. As the aim was to measure the transparency, the colour difference to the pattern (ΔE*ab (D65)) was evaluated. This value must be <2 for the sample being considered the same as the pattern. Therefore, if the colour of the final object is similar to that of the substrate the coating is considered transparent. Likewise, as samples were applied on black cardboards of an L* value of about 28.70 ± 0.05, similar values for the final applications were expected. As observed, there were no remarkable differences between the formulations. For all the studied cases, the L* values and ΔE*ab (D65) values smaller than 30 and 2, respectively, were obtained. Therefore, all the formulations were highly transparent.

The gloss results for the formulations applied at different surfaces are shown in Table S3. In dark glass a decrease in the reflected light was observed when phosphorous compounds were incorporated into the polymeric chain, even though the surface was still considered to be highly reflective. Similar results were obtained by F. Çelebi et al. when phosphorous phenyl dihydroxy was incorporated to the polyurethane chain [46]. The decrease in gloss was attributed to the higher surface roughness provoked by the particles and aggregates [47]. Therefore, it could be concluded that the phosphorous compounds made the particles aggregates, which was in agreement with the results discussed above. When the formulations were applied on wood, either sapele or oak, the gloss decreased significantly, due to the pores making the surface uneven. Hence, PU/PMMA_E50% on sapele was considered a matte coating and in the case of oak, it was close to being considered matte.

The cross-cut-adhesion test results of the formulations on different substrates are summarised on Table S4 and Fig. S6. For PU/PMMA and PU/PMMA_E50%, the adhesion of the coating to wood was maximum and no separation was observed. The hydrogen bonds between the urethane moieties and the hydroxyls of the wood substrates contributed to good adhesion strength [48]. However, for PU/PMMA_S10% this property decreased slightly, concluding that cross-linking promoted by Sartomer restricted in some extent the creation of hydrogen bonds. This agreed with the result of STEM where it was appreciated that the cross-linking of the PU was obtained where PMMA particles were dispersed.

Water sensibility was analysed by keeping water in contact with the coated surface (Fig. S7). Waterborne coatings tend to trap water by hydrophilic groups [49]. In the case of PU/PMMA, the appearance of blisters was observed, which disappeared when the sample was dried. For PU/PMMA_S10%, a slightly whitish colour was observed, which also disappeared on drying. Both cases were demonstrations of water absorption. When Exolit was incorporated to the chain, since it contained hydrophilic polyethylene oxide segments, the film was destroyed after
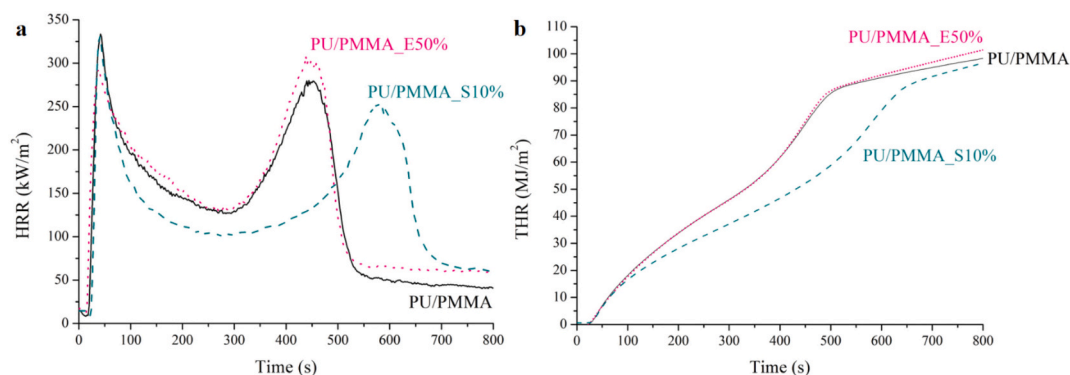
Fig. 10. a) Heat release rate and b) total heat release rate measured by cone calorimetry.

Table 8
Cone calorimetry data obtained for different formulations.

Samples	P [wt%]	TTI [s]	THR [MJ·m^{-2}]	EHC [MJ·kg^{-1}]	pHRR [kW·m^{-2}]	TT pHRR [s]	pHRR [kW·m^{-2}]	TT pHRR [s]	Residue [%]	tCO [kg/kg]	tCO$_2$ [kg/kg]
PU/PMMA	–	21.5	109.3	14.4	319.9	43	270.8	440	16.2	0.03	1.3
PU/PMMA_E50%	1.17 ± 0.10	18.5	115.3	14.8	278.1	40	290.8	430	15.8	0.03	1.3
PU/PMMA_S10%	0.55	23.3	107.0	14.1	311.4	38	185.2	582	19.4	0.04	1.2

water contact.

Hardness was measured by the resistance the film makes when load is applied. This resistance restrained the indenter point from penetrating as shown in Fig. S8. Consequently, the film that did not allow the indenter to penetrate was the hardest and the one that allowed penetration was the softness. According to the hardness results displayed in Table S5, when Exolit was incorporated into the chain, an increase in film hardness was observed. This effect was attributed to the decrease in polycaprolactone diol content, which contributed to the soft segment of the polyurethane. So, in this sample a part of the PCL was replaced by Exolit, a lower molar mass diol that makes the obtained film harder [50]. On the other hand, when Sartomer was incorporated the hardness did not show significant changes.

Cone calorimetry was used to study the fire behaviour of the formulated coatings. As the formulations were applied on wood particle board substrates when HRR was analysed as a function of time (see Fig. 10a), the characteristic wood double peak was appreciated. The first peak, before carbonisation and the second one, at the end of the test, was related to the char cracking or to the increase of the pyrolysis efficiency [41]. The fire-retardant contribution requires the smoothing of these two peaks to obtain two broad peaks of smaller area, which means a significant reduction in HRR [51]. Therefore, a decrease in THR was expected, although the phosphorus amount was not large enough to maintain its effect in the condensed-phase.

For Exolit containing samples, the influence of phosphorus on TTI, THR, EHC, pHRR and final residue content was observed (see Table 8). The decrease in the time to ignition, when phosphorus was incorporated into the polymeric chain, confirmed that phosphorus required less energy to be released. As for pHRR data obtained, from PU/PMMA to PU/PMMA_E50% a decrease of 13 % for the first peak and an increase of 7 % for the second peak was appreciated. On this basis, it could be concluded that phosphorus could act on the fire combustion process in its early stages, although this effect could not be sustained over time, resulting in the increase of the heat released in later stages. Therefore, it could be said that phosphorus was not able to generate the carbonaceous layer, so there was no improvement regarding THR, EHC and final residue quantity [17,19]. In addition to heat, released CO and CO$_2$ were also recorded (tCO and tCO$_2$ respectively), but they did not show any improvement with the addition of phosphorus. However, a remarkable diminution of the peak of both gases was appreciated. Furthermore, the

maximum peak occurred at higher times. Considering this, the action of the phosphorus as flame retardant was effective but the amount in the prepared samples was not high enough.

In the Sartomer containing samples, in terms of released heat no significant changes could be appreciated in the characteristic first peak of the wood (decrease of 3 %). However, the main differences occurred once this peak occurred, since there was a significant delay (of 142 s) and decrease (of 32 %) in the second peak. This effect could be explained by the formation of the carbonaceous layer after the phosphorus release. It is worth noting that in contrast to TGA and PCFC results, the residue of the sample containing Exolit was very similar to that of pure PU while the sample containing Sartomer presented a higher residue. The origin of these differences was probably due to the higher heating rate employed in the Cone Calorimeter. [52]. Even though a delay was given in the released heat, there was no large variation on the released total amount (see Fig. 10b) and effective heat of combustion. On the other hand, for the released CO and CO$_2$, similar results to those with regard to Exolit were obtained, but in a lesser extent.

4. Conclusions

Phosphorus modified Polyurethane/acrylic hybrid dispersions were successfully obtained. Urethane and acrylic segments were phase separated but correct compatibilisation was reached when using HEMA. The introduction of phosphorus in the formulation (via polyol or acrylic phosphate) increased the particle size and promoted their aggregation giving rise to cross-linked coatings. Dispersions with high amounts of acrylic phosphate coagulated and it was not possible to obtain stable dispersions combining the phosphorylated polyol and acrylic monomer. As the phosphorus was covalently bonded, all the coatings were transparent. Dispersions were formulated as wood coatings and the cone calorimeter data showed that the action of phosphorus as fire retardant was not very noticeable. In order to reach optimal fire-resistance, the phosphorus content of the coatings should be increased, but it was not possible using the present strategy.

CRediT authorship contribution statement

M. Puyadena Research, Writing - Original Draft,
I. Etxeberria, Research.

L. Martin, Research, Supervision.

A. Mugica Research, Supervision.

A. Agirre Research, Supervision.

M. Cobos Research.

A. Gonzalez Conceptualization, Supervision.

A. Barrio Conceptualization, Supervision.

L. Irusta Conceptualization, Supervision Writing - Original Draft.

Declaration of competing interest

The authors declare that they have no known competing financial interests or personal relationships that could have appeared to influence the work reported in this paper.

Acknowledgements

Appendix A. Supplementary data

Supplementary data to this article can be found online at https://doi. org/10.1016/j.porgcoat.2022.107005.

References

[1] S. Mehravar, N. Ballard, R. Tomovska, J.M. Asua, Polyurethane / acrylic hybrid waterborne dispersions: synthesis, properties and applications, Ind. Eng. Chem. Res. 58 (2019) 20902–20922, https://doi.org/10.1021/acs.iecr.9b02324.

[2] C.R. Hegedus, K.A. Kloiber, A. Products, Aqueous acrylic-polyurethane hybrid dispersions and their use in industrial coatings, J. Coat. Technol. 68 (1996) 39–48.

[3] H. Sardon, L. Irusta, M.J. Fernández-Berridi, J. Luna, M. Lansalot, E. Bourgeat-Lami, Waterborne polyurethane dispersions obtained by the acetone process: a study of colloidal features, J. Appl. Polym. Sci. 120 (2011) 2054–2062, https://doi.org/10.1002/app.33308.

[4] A.K. Nanda, D.A. Wicks, The influence of the ionic concentration, concentration of the polymer, degree of neutralization and chain extension on aqueous polyurethane dispersions prepared by the acetone process, Polymer (Guildf). 47 (2006) 1805–1811, https://doi.org/10.1016/j.polymer.2006.01.074.

[5] J.M. Asua, Emulsion polymerization: from fundamental mechanisms to process developments, J. Polym. Sci. Part A Polym. Chem. 42 (2004) 1025–1041, https://doi.org/10.1002/pola.11096.

[6] J. Kozakiewicz, Developments in aqueous polyurethane and polyurethane-acrylic dispersion technology Part II Polyurethane-acrylic dispersions and modification of polyurethane and polyurethane-acrylic dispersions, Polymers 61 (2016) 81–91, https://doi.org/10.14314/polimery.2016.081.

[7] S. Mehravar, N. Ballard, A. Veloso, R. Tomovska, J.M. Asua, Toward a green synthesis of Polyurethane/(Meth)acrylic dispersions through control of colloidal characteristics, Langmuir 34 (2018) 11772–11783, https://doi.org/10.1021/acs.langmuir.8b02264.

[8] Y. Lu, R.C. Larock, New hybrid latexes from a soybean oil-based waterborne polyurethane and acrylics via emulsion polymerization, Biomacromolecules 8 (2007) 3108–3114, https://doi.org/10.1021/bm700522z.

[9] S. Mehravar, N. Ballard, A. Agirre, R. Tomovska, J.M. Asua, Role of grafting on particle and film morphology and film properties of zero VOC polyurethane/poly (meth)acrylate hybrid dispersions, Macromol. Mater. Eng. 304 (2019) 1–10, https://doi.org/10.1002/mame.201800532.

[10] S. Mehravar, K.J. Roschmann, P.U. Arocha, B. Reck, A. Agirre, R. Tomovska, J. M. Asua, N. Ballard, Correlating microstructure and performance of PU/(meth) acrylic hybrids as hardwood floor coating, Prog. Org. Coat. 131 (2019) 417–426, https://doi.org/10.1016/j.porgcoat.2019.03.002.

[11] J. Wang, H. Wu, R. Liu, L. Long, J. Xu, M. Chen, H. Qiu, Preparation of a fast water-based UV cured polyurethane-acrylate wood coating and the effect of coating amount on the surface properties of oak (Quercus alba L.), Polymers (Basel) 11 (2019), https://doi.org/10.3390/polym11091414.

[12] L. Lowden, T. Hull, Flammability behaviour of wood and a review of the methods for its reduction, Fire Sci. Rev. 2 (2013) 4, https://doi.org/10.1186/2193-0414-2-4.

[13] Z. Xu, Z. Chu, L. Yan, Enhancing the flame-retardant and smoke suppression properties of transparent intumescent fire-retardant coatings by introducing boric acid as synergistic agent, J. Therm. Anal. Calorim. 133 (2018) 1241–1252, https://doi.org/10.1007/s10973-018-7201-3.

[14] H. Qiao, Y. Liang, G. Xu, Y. Wang, J. Yang, J. Hu, Preparation, characterization and flame retardancy of phosphorus-containing poly-styrene-acrylate emulsion, Des.

[15] F. Tabatabaee, M. Khorasani, M. Ebrahimi, A. González, L. Irusta, H. Sardon, Synthesis and comprehensive study on industrially relevant flame retardant waterborne polyurethanes based on phosphorus chemistry, Prog. Org. Coat. 131 (2019) 397–406, https://doi.org/10.1016/j.porgcoat.2019.02.042.

[16] T. Jang, H.J. Kim, J.B. Jang, T.H. Kim, W. Lee, B. Seo, W.B. Ko, C.S. Lim, Synthesis of waterborne polyurethane using phosphorus-modified rigid polyol and its physical properties, Polymers (Basel) 13 (2021) 1–9, https://doi.org/10.3390/polym13030432.

[17] L. Gu, Y. Luo, Flame retardancy and thermal decomposition of phosphorus-containing waterborne polyurethanes modified by halogen-free flame retardants, Ind. Eng. Chem. Res. 54 (2015) 2431–2438, https://doi.org/10.1021/ie5045692.

[18] J. Feng, Z. Ge, C. Chai, S. Wang, D. Yu, G. Wu, Y. Luo, Flame retardant modification of waterborne polyurethane fabric coating agent with high hydrostatic pressure resistance, Prog. Org. Coat. 97 (2016) 91–98, https://doi.org/10.1016/j.porgcoat.2016.03.020.

[19] J. Zhu, J. Li, W. Cai, Y. Luo, Synthesis and application of a phosphorus-containing waterborne polyurethane based polymeric dye with excellent flame retardancy, Prog. Org. Coat. 140 (2020), 105525, https://doi.org/10.1016/j.porgcoat.2019.105525.

[20] S. Rattanapan, P. Pasetto, J.F. Pilard, V. Tanrattanakul, Preparation and properties of bio-based polyurethane foams from natural rubber and polycaprolactone diol, J. Polym. Res. 23 (2016), https://doi.org/10.1007/s10965-016-1081-7.

[21] M. Schappacher, N. Fur, S.M. Guillaume, Poly(methyl methacrylate)-poly (caprolactone) AB and ABA block copolymers by combined ring-opening polymerization and atom transfer radical polymerization, Macromolecules 40 (2007) 8887–8896, https://doi.org/10.1021/ma070417q.

[22] X. Feng, G. Li, Catalyst-free β-hydroxy phosphate ester exchange for robust fire-proof vitrimers, Chem. Eng. J. 417 (2021), 129132, https://doi.org/10.1016/j.cej.2021.129132.

[23] S. Mehravar, N. Ballard, R. Tomovska, J.M. Asua, The influence of macromolecular structure and composition on mechanical properties of films cast from solvent-free Polyurethane/Acrylic hybrid dispersions, Macromol. Mater. Eng. 304 (2019) 1–10, https://doi.org/10.1002/mame.201900155.

[24] M. Rikukawa, D. Inagaki, K. Kaneko, Y. Takeoka, I. Ito, Y. Kanzaki, K. Sanui, Proton conductivity of smart membranes based on hydrocarbon polymers having phosphoric acid groups, J. Mol. Struct. 739 (2005) 153–161, https://doi.org/10.1016/j.molstruc.2004.04.034.

[25] S. Matsumura, A.R. Hlil, C. Lepiller, J. Gaudet, D. Guay, Z. Shi, S. Holdcroft, A. S. Hay, Stability and utility of pyridyl disulfide functionality in RAFT and conventional radical polymerizations, J. Polym. Sci. Part A Polym. Chem. 46 (2008) 7207–7224, https://doi.org/10.1002/pola.

[26] Y.X. Peng, Z.H. Zheng, X. Bin Ding, W.C. Zhang, Z.H. Ye, Nanometer polymer latex dispersion and its application in water-based coating, Prog. Org. Coat. 48 (2003) 161–163, https://doi.org/10.1016/S0300-9440(03)00103-6.

[27] D.E. Fiori, D.A. Ley, R.J. Quinn, Effect of particle size distribution on the performance of two-component waterreducible acrylic polyurethane coatings using tertiary polyisocyanate crosslinkers, J. Coat. Technol. 72 (2000) 63–69, https://doi.org/10.1007/bf02698006.

[28] S. Desai, I.M. Thakore, A. Brennan, S. Devi, Thermomechanical properties and morphology of interpenetrating polymer networks of polyurethane-poly(methyl methacrylate), J. Appl. Polym. Sci. 83 (2002) 1576–1585, https://doi.org/10.1002/app.10135.

[29] S. Peng, Y. Jin, T. Sun, R. Qi, B. Fan, X. Cheng, Synthesis of high solid content waterborne polyurethanes with controllable bimodal particle size distribution, J. Appl. Polym. Sci. 131 (2014) 1–9, https://doi.org/10.1002/app.40420.

[30] K. Mequanint, R. Sanderson, Nano-structure phosphorus-containing polyurethane dispersions: synthesis and crosslinking with melamine formaldehyde resin, Polymer (Guildf). 44 (2003) 2631–2639, https://doi.org/10.1016/S0032-3861(03)00154-X.

[31] C. Yang, U. Tartaglino, B.N.J. Persson, Influence of surface roughness on superhydrophobicity, Phys. Rev. Lett. 97 (2006) 1–4, https://doi.org/10.1103/PhysRevLett.97.116103.

[32] F. Tabatabaee, M. Khorasani, M. Ebrahimi, A. González, L. Irusta, H. Sardon, Synthesis and comprehensive study on industrially relevant flame retardant waterborne polyurethanes based on phosphorus chemistry, Prog. Org. Coat. 131 (2019) 397–406, https://doi.org/10.1016/j.porgcoat.2019.02.042.

[33] A. Santamaria-Echart, A. Arbelaiz, A. Saralegi, B. Fernández-d'Arlas, A. Eceiza, M. A. Corcuera, Relationship between reagents molar ratio and dispersion stability and film properties of waterborne polyurethanes, Colloids Surfaces A Physicochem. Eng. Asp. 482 (2015) 554–561, https://doi.org/10.1016/j.colsurfa.2015.07.012.

[34] X. Jiang, J. Li, M. Ding, H. Tan, Q. Ling, Y. Zhong, Q. Fu, Synthesis and degradation of nontoxic biodegradable waterborne polyurethanes elastomer with poly (ε-caprolactone) and poly(ethylene glycol) as soft segment, Eur. Polym. J. 43 (2007) 1838–1846, https://doi.org/10.1016/j.eurpolymj.2007.02.029.

[35] S.W. Kuo, H.C. Kao, F.C. Chang, Thermal behavior and specific interaction in high glass transition temperature PMMA copolymer, Polymer (Guildf). 44 (2003) 6873–6882, https://doi.org/10.1016/j.polymer.2003.08.026.

[36] S.M. Cakić, M. Špírková, I.S. Ristić, J.K.B. Simendić, M.M. Cincović, R. Poręba, The waterborne polyurethane dispersions based on polycarbonate diol: effect of ionic content, Mater. Chem. Phys. 138 (2013) 277–285, https://doi.org/10.1016/j.matchemphys.2012.11.057.

[37] Q. Zhang, E.E. Remsen, K.L. Wooley, Shell cross-linked nanoparticles containing hydrolyrically degradable, crystalline core domains, J. Am. Chem. Soc. 122 (2000) 3642–3651, https://doi.org/10.1021/ja993941o.

[38] I. Zagozdzon, P. Parcheta, J. Datta, Novel cast polyurethanes obtained by using reactive phosphorus-containing polyol: synthesis, thermal analysis and combustion behaviors, Materials (Basel) 14 (2021) 2699, https://doi.org/10.13390/ma14112699.

[39] S.L. Chai, M.M. Jin, H.M. Tan, Comparative study between core-shell and interpenetrating network structure polyurethane/polyacrylate composite emulsions, Eur. Polym. J. 44 (2008) 3306–3313, https://doi.org/10.1016/j.eurpolymj.2008.07.038.

[40] S. Jiang, Y. Shi, X. Qian, K. Zhou, H. Xu, S. Lo, Z. Gui, Y. Hu, Synthesis of a novel phosphorus- and nitrogen-containing acrylate and its performance as an intumescent flame retardant for epoxy acrylate, Ind. Eng. Chem. Res. 52 (2013) 17442–17450, https://doi.org/10.1021/ie4028439.

[41] A. Yasemin, M. Doğan, E. Bayramlı, The effect of red phosphorus on the fire properties of intumescent pine wood flour – LDPE composites yasemin, Finnish-Swedish Flame Days 2009 (2009) 4B, https://doi.org/10.1002/fam.

[42] L.L. Chu, S.K. Anderson, J.D. Harris, M.W. Beach, A.B. Morgan, Styrene-acrylonitrile (SAN) layered silicate nanocomposites prepared by melt compounding, Polymer (Guildf). 45 (2004) 4051–4061, https://doi.org/10.1016/j.polymer.2004.03.012.

[43] Z. Ding, J. Li, W. Xin, Y. Luo, Facile and high-concentration exfoliation of montmorillonite into mono-layered nanosheets and application in multifunctional waterborne polyurethane coating, Appl. Clay Sci. 198 (2020), 105798, https://doi.org/10.1016/j.clay.2020.105798.

[44] B.C.K. Ly, E.B. Dyer, J.L. Feig, A.L. Chien, S. Del Bino, Research techniques made simple: cutaneous colorimetry: a reliable technique for objective skin color measurement, J. Invest. Dermatol. 140 (2020) 3–12.e1, https://doi.org/10.1016/j.jid.2019.11.003.

[45] J.R. McGrath, M. Beck, M.E. Hill, Replicating red: analysis of ceramic slip color with CIELAB color data, J. Archaeol. Sci. Rep. 14 (2017) 432–438, https://doi.org/10.1016/j.jasrep.2017.06.020.

[46] F. Çelebi, L. Aras, G. Gündüz, I.M. Akhmedov, Synthesis and characterization of waterborne and phosphorus-containing flame retardant polyurethane coatings, J. Coat. Technol. 75 (2003), https://doi.org/10.1007/bf02757863.

[47] C. Sow, B. Riedl, P. Blanchet, UV-waterborne polyurethane-acrylate nanocomposite coatings containing alumina and silica nanoparticles for wood: mechanical, optical, and thermal properties assessment, J. Coat. Technol. Res. 8 (2011) 211–221, https://doi.org/10.1007/s11998-010-9298-6.

[48] K. Wazarkar, M. Kathalewar, A. Sabnis, Improvement in flame retardancy of polyurethane dispersions by newer reactive flame retardant, Prog. Org. Coat. 87 (2015) 75–82, https://doi.org/10.1016/j.porgcoat.2015.05.016.

[49] M. Dai, J. Wang, Y. Zhang, Improving water resistance of waterborne polyurethane coating with high transparency and good mechanical properties, Colloids Surf. A Physicochem. Eng. Asp. 601 (2020), 124994, https://doi.org/10.1016/j.colsurfa.2020.124994.

[50] V. García-Pacios, J.A. Jofre-Reche, V. Costa, M. Colera, J.M. Martín-Martínez, Coatings prepared from waterborne polyurethane dispersions obtained with polycarbonates of 1,6-hexanediol of different molecular weights, Prog. Org. Coat. 76 (2013) 1484–1493, https://doi.org/10.1016/j.porgcoat.2013.06.005.

[51] M. Gao, J. Niu, R. Yang, Synergism of GUP and boric acid characterized by cone calorimetry and thermogravimetry, J. Fire Sci. 24 (2006) 499–511, https://doi.org/10.1177/0734904106061522.

[52] Y.H. Ng, I.S. Zope, A. Dasari, K.H. Tan, Correlating the performance of a fire-retardant coating across different scales of testing, Polymers (Basel) 12 (2020) 1–19, https://doi.org/10.3390/polym12102271.